10-13-2010

Effects of open and closed system oxidation on texture and magnetic response of remelted basaltic glass

Katherine Burgess
Brown University, katherine_burgess@brown.edu

Reid F. Cooper
Brown University

Julie A. Bowles
University of Wisconsin-Milwaukee, bowlesj@uwm.edu

Jeffrey S. Gee
University of California - San Diego, jsgee@ucsd.edu

Daniele J. Cherniak
Rensselaer Polytechnic Institute

Geochemistry Geophysics Geosystems G3

Article
Volume 11, Number 10
13 October 2010
Q10007, doi:10.1029/2010GC003248
ISSN: 1525-2027

Published by AGU and the Geochemical Society

Effects of open and closed system oxidation on texture and magnetic response of remelted basaltic glass

Katherine Burgess and Reid F. Cooper
Department of Geological Sciences, Brown University, Providence, Rhode Island 02912, USA (katherine_burgess@brown.edu)

Julie A. Bowles
Institute for Rock Magnetism, University of Minnesota–Twin Cities, Minneapolis, Minnesota 55455, USA

Jeffrey S. Gee
Scripps Institution of Oceanography, University of California, San Diego, La Jolla, California 92093, USA

Daniele J. Cherniak
Department of Earth and Environmental Sciences, Rensselaer Polytechnic Institute, Troy, New York 12180, USA

[1] As part of an experimental and observational study of the magnetic response of submarine basaltic glass (SBG), we have examined, using ion backscattering spectrometry (RBS), transmission and scanning electron microscopy, energy dispersive X-ray spectrometry, and surface X-ray diffraction, the textures wrought by the controlled, open and closed system oxidation of glasses prepared by the controlled environment remelting and quenching of natural SBG. Initial compositions with ~9 wt % FeO* were melted at 1430°C with the oxygen fugacity buffered at fayalite-magnetite-quartz; melts were cooled at a rate of 200°C min^{-1} near the glass transition (T_g = 680°C). In open system experiments, where chemical exchange is allowed to occur with the surrounding atmosphere, polished pieces of glass were reheated to temperatures both below and above T_g for times 1–5000 h; undercooled melts were oxidized at 900°C and 1200°C for 18 and 20 h, respectively. RBS demonstrates unequivocally that the dynamics of open system oxidation involves the outward motion of network-modifying cations. Oxidation results in formation of a Fe-, Ca-, and Mg-enriched surface layer that consists in part of Ti-free nanometer-scale ferrites; a divalent-cation-depleted layer is observed at depths >1 μm. Specimens annealed/oxidized above T_g have magnetizations elevated by 1–2 orders of magnitude relative to the as-quenched material; this does not appear to be related to the surface oxidation. Quenched glass (closed system, i.e., no chemical exchange between sample and atmosphere) exhibits very fine scale chemical heterogeneities that coarsen with time under an electron beam; this metastable amorphous immiscibility is the potential source for the nucleation of ferrites with a wide range of Ti contents, ferrites not anticipated from an equilibrium analysis of the bulk basalt composition.

Components: 11,200 words, 7 figures, 3 tables.

Keywords: submarine basaltic glass; magnetic properties; ferrite chemistry; amorphous immiscibility; oxidation; chemical diffusion.

Index Terms: 1519 Geomagnetism and Paleomagnetism: Magnetic mineralogy and petrology; 3939 Mineral Physics: Physical thermodynamics; 8412 Volcanology: Reactions and phase equilibria (1012, 3612).

Received 4 June 2010; **Revised** 16 August 2010; **Accepted** 26 August 2010; **Published** 13 October 2010.

Burgess, K., R. F. Cooper, J. A. Bowles, J. S. Gee, and D. J. Cherniak (2010), Effects of open and closed system oxidation on texture and magnetic response of remelted basaltic glass, *Geochem. Geophys. Geosyst.*, *11*, Q10007, doi:10.1029/2010GC003248.

1. Introduction

[2] Submarine basaltic glass (SBG) has been identified as particularly useful in paleointensity studies [*Pick and Tauxe*, 1993, 1994; *Tauxe*, 2006, and references therein] due to its ideal behavior in Thellier-type experiments. The dominant (paleo) magnetic carrier in SBG is submicrometer, low-Ti, single domain (SD) titanomagnetite [*Pick and Tauxe*, 1994]; in addition a strong superparamagnetic (SP) component is evident in hysteresis data [e.g., *Pick and Tauxe*, 1993; *Bowles et al.*, 2005]. Debate about the origin and timing of formation of the nanometer-scale phase, due to its nonequilibrium composition, is ongoing [e.g., *Heller et al.*, 2002], and we have prepared samples for an experimental and observational study in an attempt to understand both open and closed system processes occurring in the creation and evolution of basaltic glass.

[3] In order for the paleointensity experiments to accurately reproduce the intensity of the ambient field, the magnetic carrier must be a liquidus phase and/or form at high temperatures during cooling, thus carrying a thermal remanent magnetization (TRM). Later formation or growth of the phase at constant temperatures below the Curie temperature (T_c) would result in a chemical remanence (CRM), or a thermochemical remanence (TCRM) if acquired under the combined influence of chemical change and temperature decrease. A (T)CRM may be either weaker or stronger than a total TRM, depending on the temperature and mode of the chemical change [*McClelland*, 1996; *Draeger et al.*, 2006; *Yamamoto*, 2006; *Fabian*, 2009]. The low intensity recovered from glass samples relative to whole rock studies for the same time periods has led some to speculate that the remanence may not be a TRM [*Heller et al.*, 2002] though a variety of other sources for this difference are possible [*Leonhardt et al.*, 2006; *Tauxe*, 2006].

[4] Two populations of titanomagnetite have been identified in pillow basalts and glassy margins, labeled groups A and B by *Zhou et al.* [2000]. Group A grains are interpreted to crystallize in (meta)stable equilibrium from the unfractionated melt and increase in maximum size with depth from the quenched margin from ~1 μm up to tens of micrometers at a depth of several centimeters. By contrast, group B grains are found in P- and S-rich immiscible globules embedded in interstitial glass, having formed from a highly differentiated melt. They compose a very narrow size range throughout the pillow, never exceeding one micrometer along the longest axis. Tiny (tens of nm) titanomagnetite crystals found within 0.3 cm of the pillow rim and within the glassy margin are thought to be genetically related to the group A grains. In the interior of the pillow, the Ti content of the group A titanomagnetite grains is tightly grouped near the equilibrium value TM60 ($Fe_{3-x}Ti_xO_4$, where x = 0.6, or 60 mol %) for the composition and conditions of cooling; the Ti content variation near the surface is much larger, ranging to almost pure magnetite, which is not an equilibrium phase in basalts containing Ti near the fayalite-magnetite-quartz buffer [*Buddington and Lindsley*, 1964]. *Zhou et al.* [2000] find a wide compositional spread in group B grains similar to that of the near-surface group A grains. Most paleointensity studies which use SBG focus on the small grains in the glassy margin, where cooling rates near the glass transition (T_g) range from ~10 to ~330°C min^{-1} [*Bowles et al.*, 2005]. The transition is a kinetic one, and its temperature within a single composition depends on cooling rate [*Dingwell and Webb*, 1989, 1990], but the variation in T_g over the range in cooling rates found to produce glass suitable for paleointensity experiments is limited [*Wilding et al.*, 2000].

[5] Previous work with Fe-bearing silicate melts and glasses has shown the formation of nanometer-scale ferrites at and near the surface of the sample during dynamic oxidation [*Cooper et al.*, 1996a, 1996b; *Smith and Cooper*, 2000]. We explore the possibility that a similar open system process occurring in MORB during underwater eruption and cooling could lead to the formation of the titanomagnetites observed in SBG. The small titanomagnetites found by *Zhou et al.* [2000] very close to the pillow rim could be genetically unrelated to both group A and group B, instead forming through open system dynamic oxidation processes.

[6] When melt or glass equilibrated at relatively low f_{O_2} is brought into contact with more oxidizing conditions, there are three kinetic responses (modes) to such a driving force: mode I, molecular oxygen diffuses into the material; mode II, ionic oxygen diffuses in, charge balanced by inward diffusion of electron holes, $h^{\bullet}$; and mode III, network-modifying cations diffuse out of the material to the free surface, charge balanced by an inward flux of $h^{\bullet}$. The process that dissipates the energy of the redox potential most quickly dominates the reaction dynamics. Mode III, (divalent) modifier cation diffusion-limited, is the dominant mode of oxidation in Fe-bearing basaltic and basalt-like glasses at temperatures near T_g [*Cooper et al.*, 1996a, 1996b; *Cook and Cooper*, 2000]. This case corresponds to $(c_h \cdot D_h) \gg (c_{Me^{2+}} D_{Me^{2+}}) \gg [(c_{O_2} D_{O_2}) \text{ or } (c_{O^{2-}} D_{O^{2-}})]$, where c_i is the concentration and D_i is the mobility of species i (this product, when normalized by RT, where R is the universal gas constant and T is temperature, is the transport coefficient of species i). The electron hole, structurally present as network-modifying Fe^{3+}, serves to decouple electrically the diffusion of cations from each other; thus the internal anion-cation ratio is increased through removal of cations, with incorporation of new oxygen to the system in the form of oxides at the surface.

[7] Substantial structural changes in the melt/glass are expected as a result of dynamic oxidation: the structural distortion created by the ferric iron "replacing" ferrous iron and the removal of divalent cations leads to a reaction in the glass at depth and nucleation of ferrites [*Cooper et al.*, 1996b; *Smith and Cooper*, 2000]. However, the presence of alkali cations can instead stabilize the Fe^{3+} cations as tetrahedral network formers [e.g., *Mysen and Richet*, 2005, p. 341], preventing the precipitation of the ferrite phase. In temperature range above T_g but below the liquidus, crystallization can change cation availability, but the dominant response to oxidation (i.e., cation migration) remains the same [*Burkhard and Müller-Sigmund*, 2007]. The open system oxidation of FeO-CaO-MgO-Al_2O_3-SiO_2 glass at temperatures slightly below T_g shows the formation of surface $(Mg,Fe)_3O_4$ and CaO oxide layers and interior nucleation of (magnesio)ferrites [*Smith and Cooper*, 2000], consistent with this model. By contrast, in nepheline normative tholeiitic basaltic glass oxidized near T_g, the texture included the surface oxide layer, but no ferrites were observed internally; rather a Na^+-stabilized Fe^{3+}-bearing glass was formed [*Cooper et al.*, 1996a]. The presence of alkalis in SBG, then, although in relatively low concentrations, may affect the oxidation texture and dynamics of the material.

[8] At very low temperatures, we expect alkalis to be the most mobile cation species (that is, have the greatest transport coefficient) responding to an oxidation potential, due primarily to the low activation energy for diffusion for alkalis relative to alkaline earths and other nonalkali network modifiers in silicate melts [*Lowry et al.*, 1982; *Henderson et al.*, 1985; *Chakraborty*, 1995]. Extrapolation of diffusivities in melts to below T_g is difficult because of the very different time scale of relaxation [*Dingwell*, 1990], but there is evidence nevertheless that an Arrhenius relationship is maintained at low temperatures for some glass compositions [*Roselieb and Jambon*, 2002]. This change in dynamics relative to higher temperatures would create an area in the interior of the glass depleted in alkalis, increasing the likelihood of ferrite nucleation. At these very low temperatures, however, the kinetic barriers to diffusion and crystalline nucleation and growth may be too large for characterization in laboratory experiments.

[9] Ti^{4+} fills a complicated structural role in basaltic melts and glasses that varies with composition and temperature [*Dingwell*, 1992; *Mysen and Neuville*, 1995]. There is, however, no evidence that Ti^{4+} is mobilized during redox reactions in basaltic glass [*Cooper et al.*, 1996a]. Thus, it will not move (to first order) with the monovalent and divalent cations affected by dynamic oxidation, including Fe^{2+}, and will instead remain at a constant Ti/Si ratio at all levels of the glass, leading to a low Ti/Fe in the surface and (perhaps) near surface region(s) as oxidation progresses. Subsequent crystallization in this region would have a much lower Ti/Fe ratio than expected for the bulk rock.

[10] At the time of eruption mid-ocean ridge basalts have an f_{O_2} slightly below the fayalite-magnetite-quartz (FMQ) buffer [*Christie et al.*, 1986]. The change in conditions, both temperature and oxygen fugacity, during emplacement of the submarine basalts is extreme and immediate. The incredible driving forces for both oxidation and crystallization created by this change in conditions could have large effects on the material, with the extreme disequilibrium leading to the presence of crystalline phases not generated by either equilibrium solidification or fractional solidification of the initial melt, as normally contemplated. Diffusion of cations under these conditions and at temperatures above the glass transition is fast enough to have

Table 1. Starting Material Composition (N1) and Surface (Slab 1) and Near-Surface (Slab 2) Compositions Discerned for Oxidized Glass Specimens[a]

	N1[b]			
Oxide	Weight Percent	Mole Percent	Slab 1 (wt %)	Slab 2 (wt %)
SiO_2	50.28	52.32	26.43	50.16
TiO_2	1.48	1.16	0.73	1.37
Al_2O_3	16.49	10.11	8.41	15.81
FeO[c]	9.15	7.96	13.17	8.06
MgO	8.33	12.92	11.82	7.69
MnO	0.16	0.14	0.10	0.10
CaO	11.84	13.20	32.89	8.83
Na_2O	2.07	2.09	1.14	7.84
K_2O	0.06	0.04	0.03	0.04
P_2O_5	0.15	0.06	0.05	0.10
SO_3	tr.	tr.	5.23	tr.

	N1[b]
T_g	680°C
Density[d]	2.83 g cm^{-3}
NBO/T[e]	0.711

[a]RBS spectral simulation.
[b]Wavelength dispersive X-ray spectroscopy (WDS; electron microprobe) of remelted and quenched submarine basaltic glass N1.
[c]Total iron as FeO.
[d]Following the models of *Lange and Carmichael* [1987] and of *Hormadaly* [1986].
[e]Nonbridging oxygen over tetrahedrally coordinated cations, a glass/melt polymerization index [*Mysen and Richet*, 2005, p. 111].

measurable effects on concentration to depths of micrometers over tens of hours [*Burkhard and Müller-Sigmund*, 2007].

[11] Additionally, closed system processes could lead to metastable immiscibility in the glass, leading to the formation of submicrometer titanomagnetite of broadly differing chemistry in the glassy margin in a process potentially similar to that envisioned by *Zhou et al.* [2000] for the formation of group B grains within the interstitial glass. Spinodal decomposition has been noted in quenched basaltic glass [*Minitti et al.*, 2002] and in basaltic melts [*Veksler et al.*, 2007]; clustering of Fe ions, or the segregation of Fe^{3+} from Fe^{2+}+Ti^{4+} [e.g., *Naslund*, 1983], by immiscibility during quench could lead to nonequilibrium phases and so affect magnetic characteristics.

[12] We have prepared samples of quenched and heat-treated/oxidized basaltic glasses in order to elucidate the timing and conditions of ferrite formation in the glass. We have also extended the protocol to characterize oxidized, undercooled melts. Analytical techniques employed for textural analysis include ion (Rutherford) backscattering spectrometry (RBS), transmission and scanning electron microscopy (TEM; SEM), energy dispersive X-ray spectrometry (EDS) and surface X-ray diffraction (XRD). Magnetic analyses included measurement of anhysteretic remanent magnetization (ARM) and thermal demagnetization (typically of saturation isothermal remanence) to determine unblocking temperatures.

2. Experimental Approach

[13] Our starting material N1 (Table 1) was a natural basalt dredged from the Pacific-Antarctic Ridge (courtesy of Pat Castillo). The ambient pressure liquidus temperature for N1, as determined by the thermochemical model MELTS [*Ghiorso and Sack*, 1995; *Asimow and Ghiorso*, 1998], is ~1220°C. The material was placed in an alumina crucible (5–6 mL capacity) and remelted in a controlled atmosphere, vertical muffle tube Deltech furnace ($MoSi_2$ resistance elements) at 1430°C for 3 h; the apparatus, described by *Cook and Cooper* [1999], includes an elevator system, instrumented with a thermocouple that contacts the melting crucible, that allows precise control of the location of the crucible within the furnace. The oxygen fugacity was buffered at FMQ by a reactive CO-CO_2 gas mixture (CO:CO_2 = 1:10; flow rate of 44 cm^3 min^{-1} [*Myers and Eugster*, 1983]). These melts were either (1) quenched to a glass and then subsequently analyzed and/or received an oxidation annealing treatment prior to analysis or (2) cooled

Table 2. Experimental Oxidation Conditions for Reheated Glasses and Undercooled Melts

Specimen	Temperature (°C)	Time (h)
N1-150-5000	150	5000
N1-600-5.5	600	5.5
N1-600-14.5	600	14.5
N1-600-56	600	56
N1-600-100	600	100
N1-730-5.5	730	5.5
N1-730-14.5	730	14.5
N1-730-24	730	24
N1-730-100	730	100
N1-915-4	915	4
N1-1095-1	1095	1
N1-900-18u	900	18
N1-1200-20u	1200	20

to an undercooled liquid state where they were provided an oxidation anneal prior to further cooling/quenching. Continuing, we describe first approach 1 and follow with approach 2.

[14] To quench, the sample (crucible plus melt) was lowered out of the hot zone of the furnace, but still within the controlled atmosphere of the muffle, where it reached ~800°C before the muffle was opened and the sample lowered into the ambient environment. In this way the melt was quenched rapidly to a glass within its crucible: the cooling rate through the glass transition (the endotherm in differential thermal analysis (DTA: argon, 10°C min^{-1}) determined the glass transition temperature of N1 to be T_g = 680°C) was estimated to be 200°C min^{-1}. Wavelength dispersive X-ray spectroscopy (WDS) analysis, performed on a Cameca SX100 electron microprobe, from the center of the glass sample gave the starting composition reported in Table 1; the values there represent an ~0.8 wt % increase in Al_2O_3 content over the original glass composition due to reaction with the alumina crucible during remelting.

[15] The crucible was cut away from the glass using a slow speed saw. The glass within 1 mm of the crucible wall was also removed to avoid quench crystals and areas of extreme alumina contamination. TEM specimens of as-quenched glass were prepared by crushing (in alcohol) bulk glass from the center of the crucible. Glass particles were allowed to settle for several minutes, then any micrometer-scale shards still suspended at the liquid surface were scooped onto a carbon grid. TEM was done on a JEOL 2010 microscope operating at 200 keV.

[16] For open system oxidation of reheated glass, the sample was cut into pieces about 1 mm thick by several millimeters on a side, suitable for RBS analysis. One surface of each piece was polished using alumina grit to 0.3 μm. Prepared specimens were then oxidized in a horizontal muffle tube Deltech furnace in bottled air (flow rate = 25 cm^3 min^{-1}) for a range of times (1–100 h) and temperatures (600–1095°C; Table 2). One other sample was placed in a lab oven at low temperature (150°C) and allowed to react with the ambient atmosphere for seven months (5000 h). Experimental oxidation specimens are identified uniquely by oxidation temperature (in °C) and time (in h; e.g., N1-730-5.5 for the remelted/quenched natural glass subsequently oxidized at 730°C for 5.5 h).

[17] Analysis of the oxidized glass specimens was done using reflected optical microscopy, secondary electron imaging (SEI), backscattered electron imaging (BSI) and EDS in SEM, TEM, surface XRD and RBS. XRD was done on several samples within minutes of their removal from the furnace to avoid transformation of the surface nucleated crystals into amorphous hydroxides via their reaction with ambient, humid air. Oxidized samples were mounted on a conventional diffractometer (Cu-K_α radiation) such that the free surface of the sample was aligned with the source and detector optics. Specimens were scanned from 2θ = 10° to 90°, and scan times of 2.5 s per 0.02° were used. Spectra were smoothed slightly using the Savitzky-Golay algorithm. SEM/SEI and BEI were used for micrographs of cross-sectional and surface morphology. TEM cross sections preserving the oxidized surface of N1-600-100 and N1-730-100 were prepared; these were thinned to electron transparency in an ion mill (Ar^+, 15 kV).

[18] Surface imaging and analysis was complimented by compositional depth profiling with RBS, a nondestructive, chemical profiling technique that measures the energy loss of accelerated α particles (helium nuclei, He^{++}) impinging on, and backscattering from component ion nuclei of a specimen; at depth in the specimen, the α particles, too, interact with inner shell electrons. At issue are the ion-backscattering and ion-stopping cross sections (functions of both specimen composition and the kinetic energy of the α particles): each component element directly and characteristically affects the momentum loss of α particles that scatter off its nuclei while bonding between ions has no effect, thus allowing direct correlation between energy of the rebounding α particle and composition of the specimen [*Chu et al.*, 1978]. Compositional profiling can be done to a depth of several micrometers (with resolution ~10 nm),

limited by the inelastic interactions between the α particles and electrons. Lateral spatial resolution is limited by beam size, which is ~1 mm; spectra average over this area. In analysis of our oxidized specimens, initial α particle kinetic energies of 2.0 MeV and 3.5 MeV were used. RBS spectra were collected using the accelerator at the Ion Beam Laboratory of SUNY-Albany.

[19] RBS spectral analyses utilize a simulation approach: we employed the commercial analysis software RUMP (CGS, Inc., Ithaca, NY). Spectral simulations use known ion-stopping and ion-backscattering cross sections to generate a synthetic spectrum from a stipulated spatial distribution of atoms [*Doolittle*, 1985]; the synthetic spectrum can be evaluated statistically relative to the actual spectrum. Modeling was done by specifying a series of discrete slabs of constant composition parallel to the specimen surface. Thickness of model layers is measured in 10^{15} atoms cm^{-2}, and density calculations for the glass after simulating compositional changes are necessary to calculate depth in the sample in standard units.

[20] Pursuing approach 2, several samples were not quenched but rather were quickly lowered to 900°C or 1200°C and held to isothermally oxidize and crystallize for 18 and 20 h, respectively. The atmosphere was switched to bottled air immediately after lowering the sample temperature. Flow rate calculations show the furnace tube would have recycled its contents once every 1.5 min. These samples were cut and polished for microprobe analysis. Undercooled melt oxidation samples are denoted by "u" in the sample name (e.g., N1-900-18u). WDS analysis was done on polished cross sections of the specimens; RBS spectra were obtained for the free surface of N1-900-18u.

[21] Magnetic experiments were done on unoxidized samples and representative oxidized samples. Natural remanent magnetization (NRM) was measured in a 2G cryogenic magnetometer, either at the University of Hawaii Paleomagnetic Lab or the Scripps Paleomagnetic Lab. The magnetic moment of many of the glass samples was at or below the noise level of the instrument ($<10^{-10}$ Am^2); however, we were able to measure the NRM of a few of the more strongly magnetized specimens. If the NRM of the samples was primarily thermal in origin, it was acquired as the samples cooled in the presence of the ambient field in the Brown laboratory. The magnitude of this field is unknown and likely variable in both time and space. Therefore, in order to more directly compare the magnetic capacity of each sample, the samples were given an anhysteretic remanent magnetization (ARM). While not a naturally occurring remanence, the ARM is generally considered to be of a similar magnitude to a thermal remanence [*Dunlop and Özdemir*, 1997]. Prior to ARM acquisition, samples were demagnetized along all three axes in a 100 mT alternating field (AF) in the Scripps Lab. The ARM was then acquired in a 100 mT alternating field with a 100 μT bias field. To place constraints on the composition of the magnetic phase(s) in the bulk glass, a saturation isothermal remanent magnetization (IRM) acquired in a 1 T field was stepwise thermally demagnetized in air at the Institute for Rock Magnetism at the University of Minnesota. Magnetization versus applied field (magnetic hysteresis) was measured up to 1.4 T on a vibrating sample magnetometer at the Institute for Rock Magnetism.

3. Experimental Results

3.1. As-Quenched Glass: TEM Analysis

[22] At a resolution of ~30 nm in low-magnification TEM, the as-quenched glass is homogeneous. In high-magnification TEM, however, uniform amorphous immiscibility is evident, as well as the presence of nanocrystals, although these are very sparsely distributed (Figure 1). Modest energy input, i.e., from the electron beam, coarsens the emulsion. On first viewing, i.e., directly after moving the sample area into the electron beam, most of the glass appears uniform, although in some areas light and dark contrast, due to density differences, is evident at the ~1 nm scale (Figure 1a). After several minutes' exposure to the beam, there is recognizable coarsening, throughout the imaged area, which continues with time (Figure 1b); the dynamic response and the resultant texture is evidence of spinodal decomposition of the glass [*Andreev et al.*, 1984]. Electron diffraction confirms the material is entirely amorphous in these two-phase regions (Figure 1b, inset).

[23] In broadly scattered locations, diffraction patterns show the presence of nanocrystalline material (Figure 1c). In places, the pattern indicates the presence of several crystals in close proximity contributing to the pattern, but other areas have single crystal diffraction patterns. The diffraction patterns are not straightforwardly indexed, but nevertheless do indicate the presence of a phase with cubic symmetry, e.g., a ferrite.

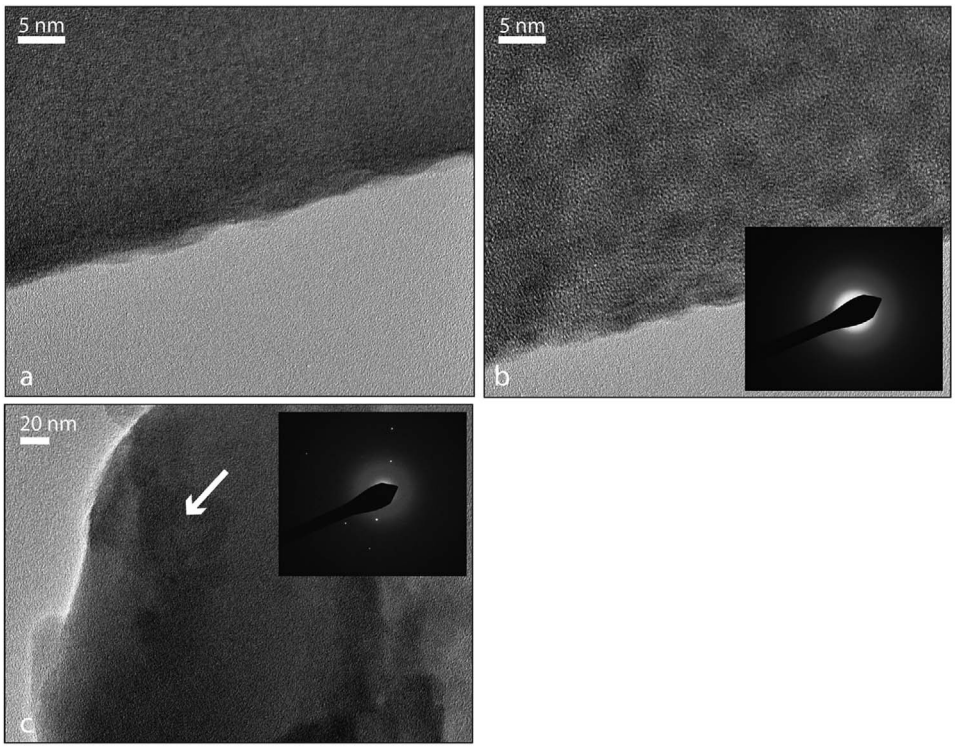

Figure 1. TEM micrographs of as-quenched basaltic glass. (a) There is a transmission density difference ~1 nm scale evident in the glass immediately after exposure to the electron beam, evidence of incipient phase separation. (b) Same area as in Figure 1a after 9 min exposure to the electron beam: the glass is clearly no longer homogeneous, instead exhibiting a texture associated with spinodal decomposition. Inset shows amorphous selected area diffraction (SAD) pattern. (c) Quenched glass with ~40 nm cubic grain present (arrow). Inset shows a SAD pattern for a cubic crystal.

3.2. Oxidized Glasses and Undercooled/ Crystallizing Melts

3.2.1. Visual Inspection and Microscopy of Oxidized Glasses and Undercooled Melts

[24] When removed from the oxidation furnace, samples oxidized at temperatures above T_g developed a lustrous/iridescent finish ranging from purple to bluish-green, while samples oxidized at lower temperatures did not. Optical microscopy and SEM revealed small individual crystals present on the surface of the lower-temperature samples, with spacing between crystals changing with oxidation annealing time, while the high-temperature samples annealed for more than 5.5 h had ~5-μm-scale surface roughness (undulation) that included a uniform coverage of a ~100-nm-scale phase(s), a complete change from the original polished surface.

[25] At least two populations of crystals are present on surface of glasses oxidized at 600°C for all anneal times, one phase rich in Fe and Mg with diameters on the order of 0.1 μm and having a cubic habit, one phase rich in Ca and S and ~2 μm across. (Chemical concentrations are discerned using EDS.) The larger crystals are euhedral to subhedral. In some cases, the larger crystals appear to be breaking down, possibly becoming amorphous with exposure to the humid, ambient environment (Figure 2a). By annealing times of 100 h, crystals cover the entire surface of the glass, and the two size range populations have grown over and into one another.

[26] In glasses oxidized at 730°C for any length of time, the surface has been entirely covered in new crystalline material. At least two different types of crystals are again recognizable, although the spacing between individuals is much closer than in the lower temperature anneal, and the surface has an undulating texture (Figure 2b). SEM images from cross sections of sample N1-730-100 show some devitrification in the center of the sample, starting at a depth of ~100 μm from the surface. Oxidation appears to have affected the specimen to a depth of 6–8 μm, and clusters of spherulitic microcrystals, likely pyroxene, have formed in this region close to the surface (Figure 2c).

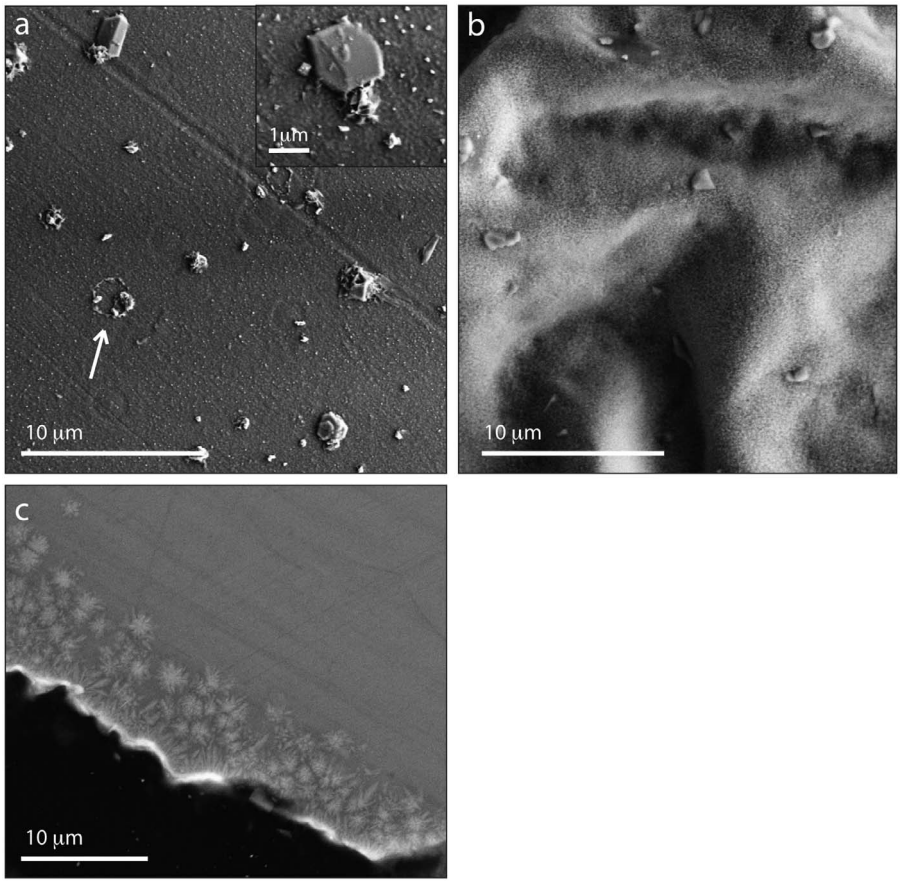

Figure 2. SEM/SEI micrographs of the oxidized, free (originally polished) surfaces of (a) N1-600-56 and (b) N1-730-24. The large, micrometer-scale crystals in both images are S- and Ca-rich; the small (~100 nm) crystals are Mg- and Fe-rich. Much more crystallization has taken place on the high-temperature sample, but the scales of the phases are similar. The arrow in Figure 2a points to a crystal reacting with the humid ambient environment; the inset is higher magnification of a euhedral crystal, also showing cubic ferrites. (c) A cross section of sample N1-730-100. The bright edge indicates the Fe and other heavy cation enrichment at the specimen free surface as a result of oxidation. Fe-rich crystalline spherules have grown in the glass up to 10 μm from the surface; this "coarse, near-surface" devitrification causes the ~5-μm-scale surface undulations evident in Figure 2b. The spherulitic growth, probably of pyroxene, is indicative of but sparse internal nucleation of ferrite due to the oxidation treatment [cf. *Beall and Rittler*, 1976; *Cooper et al.*, 1996a].

[27] Glass samples N1-915-4 and N1-1095-1 exhibit even higher degrees of devitrification in their interiors, as well as layers at the surface, more than 2 μm thick, that are very enriched in iron, although the exact depth of cation enrichment is difficult to determine from EDS due to the high degree of crystallization. N1-1095-1 is dark purple under visual inspection, and SEM imaging shows the entire surface to be covered in "rosettes" of euhedral crystals, preliminarily identified as hematite based on tabular hexagonal habit. N1-915-4 is also highly crystalline on its surface, with two distinct crystal populations, closely resembling the surface texture of N1-730-24 (Figure 2b).

[28] No ferrites were seen in TEM cross sections of the surface and near-surface region of N1-600-100. Some crystalline material, likely pyroxene, was present in N1-730-100, but there was no evidence of the densely ubiquitous, internally nucleated ferrites like those seen by *Smith and Cooper* [2000] for synthetic glasses of similar polymerization to, and $Fe^{2+,3+}$ content of, basaltic glass but containing no alkali cations.

[29] Samples isothermally oxidized and crystallized from undercooled melts (i.e., those not first quenched to a glass and then reannealed) have large pyroxenes and plagioclase crystals, in addition to spinels, both Fe- and Al-rich. Some are titanomagnetite, with Ti content approaching the equilibrium value for the composition, TM60, as determined by WDS. Irregular quench textures are present in the glassy region of N1-900-18u; crys-

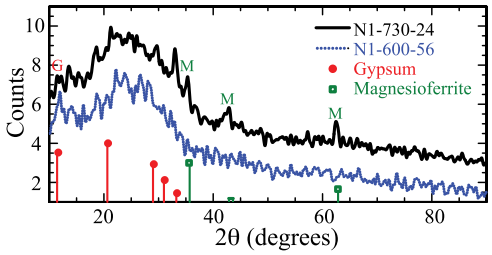

Figure 3. XRD (Cu-K_α) spectra from originally polished and then oxidized surfaces for glass specimens N1-730-24 (black solid line) and N1-600-56 (blue dotted line; offset for clarity). An amorphous hump is present between $2\theta = 15°$ and 35°. The peak at $2\theta = 11.8$ is associated with gypsum (G; $CaSO_4{\cdot}2H_2O$). Magnesioferrite to magnetite (M; $MgFe_2O_4$-Fe_3O_4) peaks are at 33.2°, 35.6°, 43°, and 62.3°.

talline textures closely resemble those seen by *Hammer* [2006] in experiments done at oxidizing conditions for various degrees of undercooling.

3.2.2. Surface XRD of Oxidized Glass Specimens

[30] In XRD spectra of polished but unoxidized glass, the sole diffraction signal is a hump associated with amorphous silicate from $2\theta = 15°$ to 35°. In N1-600-56, the hump remains dominant, but is overlain by several diffraction peaks associated with gypsum ($CaSO_4{\cdot}2H_2O$), and possibly with brucite or portlandite ($Mg(OH)_2$ and $Ca(OH)_2$, respectively), while N1-730-24 shows, too, clear diffraction peaks associated with an iron oxide phase, between magnetite (Fe_3O_4) and magnesioferrite ($MgFe_2O_4$) in composition, in addition to peaks identified as gypsum (Figure 3). These data support the EDS observations of the coarser precipitates, which show sulfur present on the surface spatially related specifically to Ca, as well as observations of the fine-particle film, enriched in Fe. When the N1-730-24 specimen was analyzed in XRD again, after being stored at room temperature in a passive desiccator for several days, the primary peak associated with gypsum decreased in intensity, consistent with its being transformed to the amorphous state, while those for the Fe oxide peaks did not.

3.3. RBS

[31] RBS spectra obtained for glasses oxidized at 600°C are presented in Figure 4a. Qualitatively, the effects of oxidation are quite striking. In comparison to unoxidized glass, there are notable increases in Fe and Ca at the free surface. The Fe peak does not grow in height with time, but the thickness of

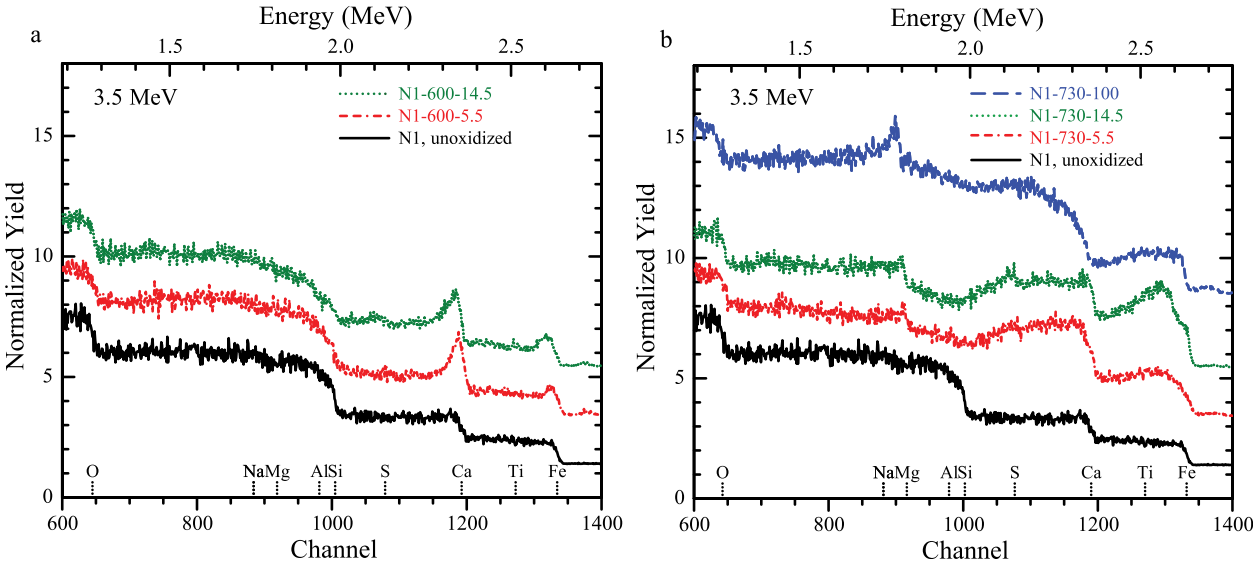

Figure 4. RBS spectra acquired at 3.5 MeV for (a) N1 samples oxidized at 600°C and (b) N1 samples oxidized at 730°C for various anneal times; in each plot, the spectrum for unoxidized glass is shown for comparison. The spectra are offset for clarity. For the 600°C oxidation (Figure 4a), note the peaks at the Fe (2.65 MeV) and Ca (2.35 MeV) edges and their change in width with oxidation time; note too that the Si edge (2.0 MeV) is tilted, indicating there is some Si present at the oxidized surface, but much has been buried by phases rich in Ca, Fe, and O. For the 730°C oxidation (Figure 4b), one sees the enhanced mobilization of Fe and Mg to the surface compared to Ca, the clear evidence of S mobilization to the surface, and the Si edge essentially buried by the Ca-, Fe-, Mg-, O-, and S-bearing phases.

Table 3. Thickness of Surface/Near-Surface Compositional Slabs for N1 Glass Oxidized at 600°C

Anneal Time (h)	Thickness[a] (10^{15} atoms cm^{-2} (nm)) Slab 1 (at the Very Surface)	Slab 2 (Me^{2+} Depleted)
5.5	500 (56)	4800 (619)
14.5	750 (83)	7300 (941)
56	1200 (133)	14000 (1804)
100	1700 (189)	18500 (2385)

[a]Converted using magnetite density (slab 1) and melt/glass density extrapolated to room temperature (slab 2) (following the models of *Lange and Carmichael* [1987] and of *Hormadaly* [1986]).

the Fe-enriched material does increase, as seen in the growth in width of the peak. Ca behaves similarly, but its peak is much larger. Sections of the spectrum behind the Fe and Ca peaks are lower than that for unoxidized glass, indicating depletion of Fe and Ca from a finite thickness of original glass now immediately below the enriched layer.

[32] The most effective spectral simulations were done by keeping the Al/Si, Ti/Si, Mn/Si, K/Si and P/Si ratios fairly constant, which itself is an indication of the most mobile ionic species responding to the gradient in oxygen chemical potential, i.e., the divalent network-modifier species Ca, Mg and Fe and the monovalent modifier Na. Spectral simulations indicate that troughs in both Ca and Fe content occur at the same depth. There is no shift of the Si edge, indicating the continued presence of Si on the free surface even after oxidation, that is, the crystalline material formed on the surface forms an incomplete layer. The surface material is enriched in S; a factor of four increase in Na concentration at a slight depth within the sample, specifically where Fe and Ca are depleted, is suggested by the increased counts relative to the unoxidized sample between 1.4 and 1.8 MeV in the 3.5 MeV spectrum. The depth of Na depletion is beyond the resolved depth of the RBS analysis for the acceleration energies used (~2 μm). There is also an increase in Mg at the surface, although there is no pronounced peak in the spectra. No peak is seen for Ti. The simplest, statistically sound fits for the 600°C anneal temperature employed three constant composition "slabs" (layers), slab 1 defining the composition of the free surface, slab 2 characterizing the divalent cation-depleted but Na-enriched region and slab 3 being infinitely thick and having the composition of the original glass. This approach suggests two reaction "fronts" characterize the oxidation, one front external to the (formerly) free surface and one front internal, i.e., within, the glass [cf. *Cooper et al.*, 1996a]; see section 4.2. The compositions of these slabs are presented in Table 1; the thicknesses of the slabs, in atoms cm^{-2} and converted to length following the density models of *Lange and Carmichael* [1987] and of *Hormadaly* [1986], are presented in Table 3. The thickness of slab 2 increases in a parabolic fashion with time (Figure 5 and Table 3).

[33] In spectra for glasses oxidized at 730°C (Figure 4b), large surface/near-surface enrichments are seen in Fe, Ca and Mg. The Ca edge, although present, is much less pronounced than for lower temperatures, while the Mg edge, which was not seen at all at 600°C, now has a large peak. The Si edge has been completely hidden (buried) by the other species being mobilized to the free surface from different depths. Areas of depletion of single ions are convoluted in the spectra with the enrichments and depth effects of other ions, but can be modeled for the short anneal times. RBS using α particles is unable to give information about composition of the samples to the depths affected by the oxidation after only a few hours of annealing at this temperature.

[34] When comparing the two anneal temperatures, one sees that Fe has moved to the surface much more at higher temperatures than at the lower temperatures, and that even for the same anneal

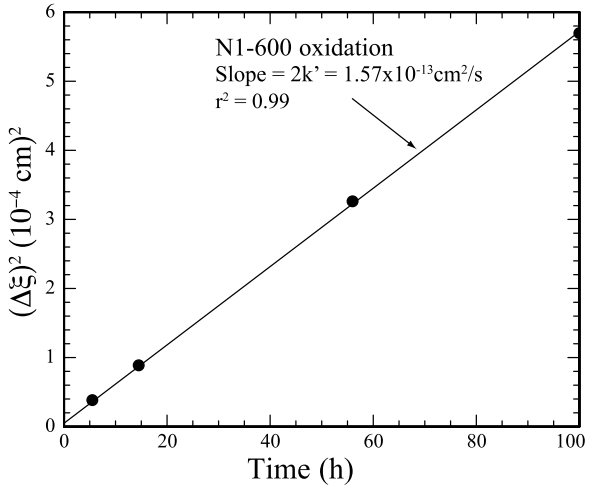

Figure 5. Thickness squared of cation-depleted region (slab 2 in Table 3) versus reaction time for glass samples oxidized at 600°C. The slope of the line is equal to $2k'$, where k' is the parabolic reaction rate constant. The linear trend indicates that the oxidation reaction is rate limited by chemical diffusion; the absolute value of k' indicates that the rate-limiting species are divalent network-modifying cations. Substitution of k' into equation (1) yields $\overline{D}_{Me^{2+}600°C} = 2.41 \times 10^{-14}$ cm^2 s^{-1}.

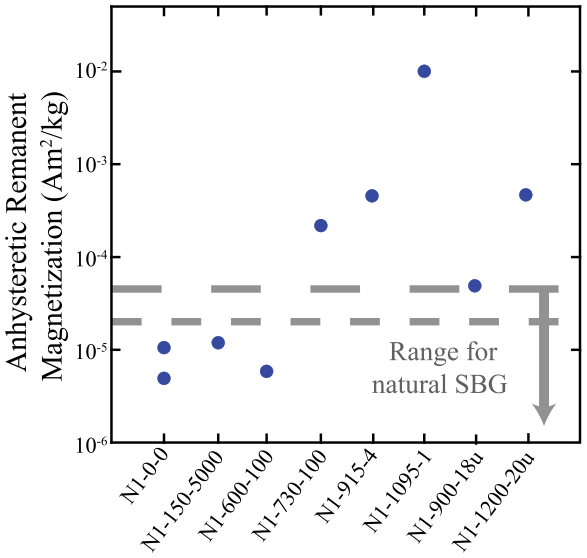

Figure 6. ARM acquired by oxidized glass and undercooled melt specimens in a 100 mT alternating field with a 100 μT bias field. Samples quenched from melt to glass (N1-0-0) have remanences comparable to those of natural SBG. Specimens oxidized below the glass transition temperature, e.g., N1-150-5000 and N1-600-100, have remanence indistinguishable from that of samples that were not reheated or reacted. Specimens that were held in air at higher temperature or allowed to crystallize in air show magnetizations elevated by 1–3 orders of magnitude. The bottom dashed line shows the upper limit for 75% of NRM data reported for natural SBG by *Bowles et al.* [2006]; the top dashed line shows the upper limit for 90% of those data (n = 459 samples).

time, the depth affected by the oxidation is much larger at temperatures above T_g.

[35] For oxidation at 150°C, even after several months annealing, the RBS spectrum shows very little change relative to the unoxidized glass. It is possible that Na (±K) could be enriched by up to a factor of three (i.e., up to several weight percent Na) without significant change to the spectrum in the region between 1.6 and 1.8 MeV, making analysis inconclusive for these cations. No other elements show significant enrichment at the free surface or depletion elsewhere.

[36] RBS spectra were obtained, too, from the oxidized undercooled melt specimens. For N1-900-18u there is a huge surface Fe peak, and an increase in Ca close to, but not at, the very surface; a significant amount of Mg is also present at the surface.

3.4. Magnetics

[37] The magnetization (ARM) acquired by the unoxidized samples is roughly in the range of the NRM of natural SBG [*Bowles et al.*, 2006]. Of the oxidized samples, only those oxidized above the glass transition show an observable increase in magnetization, while the samples oxidized at 600°C are characterized by a magnetization indistinguishable from that of samples that were not reheated (Figure 6). The increase in remanence magnitude is seen in all samples that spent time above the glass transition, whether or not they were first quenched to a glass.

[38] During thermal demagnetization of the IRM, the unoxidized glass, N1-150-5000 and N1-600-100 display continuous unblocking up to 580°C (Figure 7). In contrast, the high-T oxidized samples N1-730-100, N1-915-4 and N1-1200-20u reveal a response consistent with the development of a phase with low unblocking temperatures (<300°C), possibly high-Ti magnetite (or a ferrite incorporating some other non-Fe cation). The unblocking trends of N1-900-18u and N1-1095-1 show intermediate behavior. All samples have coercivity distributions derived from magnetic hysteresis measurements of <0.3 T, consistent with magnetite or titanomagnetite. N1-900-4 also has an additional harder phase with coercivities >0.5 T that is completely unblocked by 400°C and may be associated with titanohematite; a titanohematite surface coating on other samples is not untenable, as internal titanomagnetite could easily swamp the hematite signal.

4. Discussion

[39] *Zhou et al.* [2000] conclude that the variation in titanomagnetite composition with depth in a MORB pillow is consistent with the changes in cooling rate from rim to interior. The Ti/Fe ratio approaches the equilibrium value in slow cooling regions where thermodynamic equilibrium is possible; slow diffusion in more rapidly cooled regions limits compositions to more closely resemble the melt Ti/Fe ratio. Our data presented here show a range of textures that allow us to further elucidate the effects of cooling and chemistry on magnetic response in basaltic glass.

4.1. As-Quenched Glass: Closed System Dynamics

[40] It is clear from Figure 1 that the glass goes through (metastable) amorphous phase separation via spinodal decomposition upon quenching, with further coarsening of the texture with the input of energy from the electron beam; similar processes

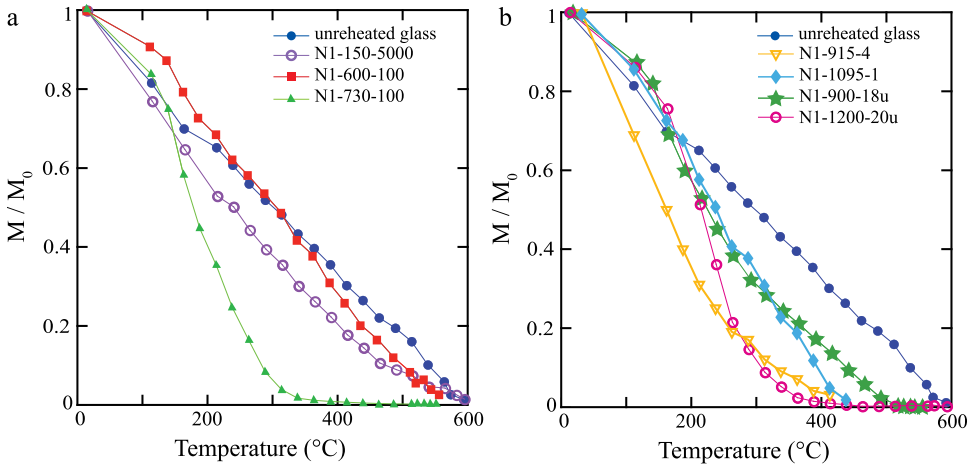

Figure 7. Thermal demagnetization of a saturation isothermal remanence (IRM). As-quenched samples display continuous unblocking up to 580°C, which, if all magnetization is attributed to crystalline ferrite, is consistent with a wide range of Ti contents, up to pure magnetite. (a) The same response occurs for glasses annealed/oxidized at temperatures up to 600°C ($<T_g$). Glass and undercooled melts oxidized at temperatures $>T_g$ show evidence for development of a phase that unblocks by ~300°C, consistent with the presence of ferrites having a moderate Ti content (>TM45). (b) The metastable extension of the immiscibility gap likely falling between samples N1-915-4 and N1-1095-1 could lead to the differences between these samples and also to the differences between the two undercooled melts, such that N1-915-4 and N1-900-18u would have undergone amorphous phase separation while N1-1095-1 would have undergone some equilibration above the metastable solvus and N1-1200-20u would not have phase separated at any point [*Visser and Koster van Groos*, 1979].

have been noted in industrial research glasses [*Seward et al.*, 1968; *Chiang and Kingery*, 1983]. Phase separation is known from glass-ceramic research to be key in controlling nucleation and composition of the nucleated phase [*McMillan*, 1979, p. 71]. As such, we suggest that the phase separation seen here and in other tholeiitic basalts [e.g., *Philpotts*, 1982] could affect the nucleation and chemistry of titanomagnetite found in SBG and lead to ferrites with the broad range of Fe/Ti ratios evidenced by the magnetic response.

[41] Average MORB compositions do not fall within the stable miscibility gap for mafic liquids [*Roedder*, 1978; *Philpotts*, 1982], but the shape of the metastable solvus extends below the liquidus to our composition [*Visser and Koster van Groos*, 1979; *Philpotts* 2008]. Liquid phase immiscibility segregates Ti^{4+} into the iron-rich liquid [*Watson*, 1976; *Visser and Koster van Groos*, 1979]; some amount of Fe will remain in the silica-rich liquid. The ferric/ferrous ratio will be higher in the silica-rich liquid because of the high proportion of alkalis that partition into this liquid and their charge balancing effect on tetrahedrally coordinated Fe^{3+} [*Mysen and Richet*, 2005, p. 341], increasing the ease of ferrite nucleation in the low-Ti liquid [*Beall and Rittler*, 1976]. Oxidation of the melt prior to or, particularly, during quenching would expand compositionally the Fe^{3+}-affected miscibility gap and, thus, the likelihood of metastable liquid phase separation [*Naslund*, 1983; *Thompson et al.*, 2007]. The amount of ferric iron can be increased solely by quenching through redox couple reactions with other heterovalent ions present in the melt, specifically $Ti^{3+,4+}$, $\pm S^{2-,4+,6+}$ [*Paul*, 1990; cf. *Cooper et al.*, 2010]. Analysis of the relative changes in the activity coefficients of the ions with temperature change shows that the relative driving force for the oxidation of Fe^{2+} versus Ti^{3+} would increase at lower temperature, leading to the oxidation to Fe^{3+} at the expense of Ti^{4+}, again facilitating the nucleation of low-Ti ferrites.

[42] The amorphous phase separation we see and the concentrating of Fe ions could have a large effect on the magnetic response of the material. In a study by *O'Horo and O'Neill* [1976], antiferromagnetically coupled Fe ions are present in quenched calcium aluminum borosilicate glass. Amorphous phase separation, evidenced in TEM imaging of the glass, is very fine scaled (<10 nm) with a morphology recognized as spinodal decomposition. They note that the separation of the glass into Fe-rich and depleted regions would enhance the possibility of clustering of the Fe ions, although

the SP blocking temperature (T_B < 4.2 K) indicates clusters less than 3 nm in diameter. Similar low-T (~2–4 K) unblocking was measured in our quenched glass specimens and in natural SBG samples. *Hayashi et al.* [1999] attribute the superparamagnetism of their iron-bearing calcium silicate glass to "microcrystalline" clusters of ~5 nm and note areas visible in TEM that indicate iron is not homogeneously distributed in the material. There is a significant stable miscibility gap within the CaO-FeO-Fe_2O_3-SiO_2 system [*Muan*, 1957; *Phillips and Muan*, 1959], suggesting that metastable immiscibility is possible upon quenching and contributes to the formation of the high-density clusters with varying Fe^{3+}/Fe^{2+}.

[43] It is possible that the spinodal decomposition in our glass, as noted in Figure 1, could lead to clustering of Fe^{3+} ions and enhanced likelihood of ferrite nucleation throughout the glass at temperatures above T_g [*O'Horo and O'Neill*, 1976], leading to the formation of the group A grains seen in the near surface region by *Zhou et al.* [2000]. A range of Ti contents would be easily obtained due to kinetic fractionation and the segregation of some iron into the silica-rich liquid, analogous to that seen in the formation of the group B grains within immiscible globules in interstitial glass.

4.2. Open System Oxidation Dynamics: Kinetics and Textural Response

[44] When basaltic glass is placed in an oxygen chemical potential gradient, the dominant mechanism of dynamic oxidation is unequivocally mode III: the high concentrations of divalent cations at and near the surface of the glass show the efficiency of this response in dissipating the energy of the driving force relative to diffusion of molecular and ionic oxygen. The observed reaction morphology of Ca-, Mg- and Fe-rich crystals grown on the surface of all samples can only occur when the diffusion of divalent cations dominates and rate limits the kinetic response to oxidation. Heat treatment alone below the glass transition, with no gradient in oxygen chemical potential, will not affect the surface and near-surface chemistry of the glass [*Cooper et al.*, 1996a].

[45] The kinetic nature of the glass transition means that over time, the molecular structure of a glass annealed at temperatures near T_g will relax, effecting a subtly different molecular structure, that is, one with a different T_g. At chemical equilibrium, this annealing-effected evolution can be characterized as a function of time and rate (i.e., dT/dt), using, e.g., differential scanning calorimetry [e.g., *Potuzak et al.*, 2008]. Open system, isothermal oxidation as pursued here, however, sees the composition of the material in the near-surface region change simultaneously with thermal relaxation, making the characterization particularly complicated. For example, evolving the chemistry of the glass from its original composition to that represented by slab 2 (Table 1), realizing that by oxidation the iron in this region is now almost entirely ferric and stabilized in a network-former role by the presence of Na^+ [*Cooper et al.*, 1996a], the glass polymerization is increased, diminishing the kinetics of mechanical/structural relaxation. Thus, the evolution of T_g of our annealed, oxidizing samples has not been quantified. Monitoring the reaction, which demonstrates parabolic kinetics, i.e., $(\Delta\xi)^2 = 2k't$, where $\Delta\xi$ is the thickness of a monitored reaction layer, t is time and k' is the parabolic reaction rate constant (Figure 5), demonstrates that the oxidation in air is rate limited by the diffusion process. We follow the model articulated by *Cooper et al.* [1996a] to determine the rate of chemical diffusion of divalent network modifiers in the glass in response to the oxidation potential. The Fick-Einstein equation is applied to analyze the fluxes of the divalent cations and electron holes as a function of the negative gradient in their electrochemical potentials, i.e., $-\nabla\eta_{Me^{2+}}$ and $-\nabla\eta_{h^{\cdot}}$, respectively. An electrochemical potential gradient for $h^{\cdot}$ cannot be sustained, however, because of their very high mobility, orders of magnitude greater than that of the cations (the "semiconductor condition"); thus, the driving force for cation diffusion is reduced to the negative chemical potential gradient for the neutral metal species, i.e., $-\nabla\mu_{Me}$. μ_{Me} in the glass/melt is related to the μ_{O_2} through the equilibrium Me + $1/2O_2$ = MeO, and since ionic diffusion across the oxidized glass internal layer (slab 2) occurs at concentration differences $X_{Me^{2+}} < 10^{-3}$, there is essentially no gradient in the μ_{MeO} across the region of oxidation; as such, $-\nabla\mu_{Me} \approx +\frac{1}{2}\nabla\mu_{O_2}$ [*Cook and Cooper*, 2000]. Thus, in transition metal oxide-bearing glasses, a chemical potential gradient in oxygen can generate a cation flux as the dominant kinetic response to oxidation (or reduction), with little or no movement of an oxygen species.

[46] An average diffusion coefficient for the divalent modifiers, $\overline{D}_{Me^{2+}}$, can be calculated for the oxidized glass, that is, for regions of the glass from which network-modifying cations were removed to form the oxide phases on the free surface, from k', which is a convolution of the ionic mobility and the

(normalized, to RT) driving force [cf. *Schmalzried*, 1983]:

$$k' = X_{Me^{2+}}\overline{D}_{Me^{2+}} \ln\left(\frac{a_{O_2}^{\xi=0}}{a_{O_2}^{\xi=\xi''}}\right), \quad (1)$$

where $X_{Me^{2+}}$ is the atomic fraction of divalent cations in the divalent cation-depleted layer (slab 2 in Table 1), a_{O_2} is oxygen activity (with the superscript indicating a specific location), ξ'' is the location of the oxidation front within the glass (the boundary between slabs 2 and 3) and $\xi = 0$ is the original surface of the glass (the boundary between slabs 1 and 2; thus, $\Delta\xi = \xi'' - 0$ and diffusion through slab 1 is treated as a short circuit in the dynamics). For $2k' = 1.57 \times 10^{-13}$ cm^2 s^{-1} (Figure 5), $X_{Me^{2+}} = 0.097$, $a_{O_2}^{\xi=0} = 0.21$ (air) and $a_{O_2}^{\xi=\xi''}$ at 600°C equal to the fayalite-magnetite-quartz (FMQ) buffer (~10^{-20} [*Myers and Eugster*, 1983]), we calculate $-\overline{D}_{Me^{2+}\ 600°C} = 1.8 \times 10^{-14}$ cm^2 s^{-1}. Our result is similar to that found by *Cooper et al.* [1996a] for the same temperature ($\overline{D}_{Me^{2+}\ 600°C} = 2.4 \times 10^{-14}$ cm^2 s^{-1}). The rapid growth of the slabs in the 730°C treatment in N1 to thicknesses greater than that seen by RBS prohibits estimation of the average diffusion coefficient with this method.

[47] In this study we see movement of alkali cations to the oxidized region of the sample at low temperatures, as was seen by *Cooper et al.* [1996a] in nepheline normative basaltic glass. The increased presence of Na^+ in the near surface region of the glass would inhibit precipitation of ferrites from the matrix. This behavior is supported by the fact that no ferrites were seen in TEM cross sections of the oxidized glass surface in the 600°C samples, in contrast to those seen by *Smith and Cooper* [2000] in oxidized glasses of similar polymerization to basalt but containing no alkali oxides. The enrichment of Na^+ in the oxidized region (slab 2) of the basaltic glass, which is otherwise depleted in network-modifying cations, and the region of Na depletion being at depths greater than that measured in RBS, is an indication of its high diffusivity within the glass, as confirmed by other workers [e.g., *Pommier et al.*, 2010]. Alkali diffusion, therefore, does not rate limit the oxidation reaction: while Na^+ participates in the dynamics, its motion is a serial kinetic step in the process overall and, too, is a short circuit compared to the motion of the divalent network modifiers; as such, chemical diffusion of Na^+ is essentially "invisible" in the kinetics.

[48] From the perspective of oxidation dynamics, sulfur is a very potent cation, having a high charge and very rapid diffusion in basalt [*Freda et al.*, 2005]. Its small size allows it to diffuse very quickly, contributing to the surface layer chemistry with extreme elevation in S concentration relative to the starting material. On the surface of oxidized glass samples, sulfur is included in (metastable) calcium silicates, as suggested by EDS chemical analyses of the large surface precipitates on the surfaces of glasses oxidized at 600 and 730°C (Figures 2a and 2b), which rapidly react to form gypsum in atmospheric conditions (Figure 3). At our experimental conditions, sulfide, sulfite and sulfate could all be present in the glass [*Métrich et al.*, 2002]. Reaction of one mole of S^{6+} at the surface of the glass is able to release more electron holes than any other cation present into the interior, contributing to the oxidation of the glass. We did not measure the concentrations of other volatiles (H_2O, CO_2) in the samples either before or after the experiments. Carbon is dissolved in basaltic glasses as carbonate complexes [e.g., *Nowak et al.*, 2003], and so would already be in an oxidized state, while hydrogen, although diffusing very rapidly, has low potency in terms of charge. While the presence of volatiles and their speciation could be important in oxidation dynamics of some natural rocks, we expect the concentrations to be very low in our samples prepared at ambient pressure and anhydrous conditions.

4.3. Magnetic Response

[49] Consistent with *Pick and Tauxe* [1994], we found no change in magnetic signature up to 600°C, where they saw the Cretaceous age sample begin to produce more magnetite as it was heated in magnetic experiments and a slight increase in magnetization in the Holocene glasses they measured. The magnetic phase was clearly present in the glass immediately after quench, a point strongly supported by experiments reported in a companion paper by J. A. Bowles et al. (manuscript in preparation, 2010). It is clear that dynamic (open system) oxidation of the basalt glasses alone does not lead to the presence of low-Ti magnetites as found in natural SBG; while diffusion may have segregated Fe from Ti, no significant nucleation of magnetic ferrites took place during low-temperature annealing and oxidation, as evidenced by the lack of difference in magnetic response between the as-quenched glass and N1-600-100. Although magnesioferrites are clearly present on the surface of the glass, the signature of the bulk, unreacted glass continues to dominate the signal. For SBG older than a few million years, reheating during

Thellier experiments could affect the magnetic response, due to devitrification of the glass over time [*Smirnov and Tarduno*, 2003]. Our experimental results show that very young glasses will not be strongly affected by such reheating until they are at temperatures above T_g.

[50] The glass oxidized at temperatures above the glass transition acquire an ARM at least an order of magnitude larger than natural glasses. The distinct change in unblocking behavior in N1-730-100 is consistent with growth of a phase rich in Ti, compared to the linear unblocking trend in as-quenched glass, which indicates that a range of titanomagnetites compositions including very low Ti magnetite is present. The presence of the near-surface pyroxene spherules evident in Figure 2c is indicative of sparse internal nucleation of ferrite in this region of the glass [*Beall and Rittler*, 1976; *Cooper et al.*, 1996a]; thus any nucleation and growth of titanomagnetite is not due to the oxidation treatment but to devitrification in the bulk glass at high temperature.

[51] It is possible to relate the magnetic responses of the undercooled melts N1-900-18u and N1-1200-20u and the high-T reheated glasses N1-915-4 and N1-1095-1 to the closed system dynamics discussed earlier. While N1-915-4 and N1-1200-20u have both increased ARM relative to natural SBG and lower unblocking temperatures, indicating a moderate to high titanium content in the dominant ferrites, N1-1095-1 and N1-900-18u have thermal unblocking spectra that fall between as-quenched glass and N1-1200-20u (Figure 7). The stable miscibility gap in basaltic melts exists to ~1110°C [*Visser and Koster van Groos*, 1979]; the metastable extension of the solvus would be well below 1200°C, making it likely that N1-1200-20u never phase separated before nucleating and growing titanomagnetites. Undercooling to below the metastable solvus allowed N1-900-18u and the quenched samples to phase separate; when brought back up to high temperature, the two amorphous phases would have coarsened, and subsequent nucleation and growth would have taken place in regions with very different Fe/Ti and alkali contents. There is increased likelihood of developing ferrites with lower Fe/Ti in the high-Fe^{2+} phase because alkalis in the low-Ti phase could inhibit ferrite nucleation. It is possible N1-730-100 went through similar phase development during annealing. Because 1095°C is likely to be above the metastable extension, any spinodal decomposition that had taken place upon quench could have reequilibrated to a single phase, leading to growth of moderately high Ti magnetite.

5. Conclusions

[52] The dynamic oxidation of basaltic glass at temperatures below and around the glass transition is due to migration of network modifying cations toward the surface of the glass in response to the oxidation potential gradient.

[53] The magnetic signature of quenched natural material is similar to that of natural SBG. Oxidation and annealing below T_g have no significant effect on the strength or nature of the magnetic response. Both results indicate that the remanence seen in SBG and our quenched experimental glass is a TRM and unrelated to open system processes. Oxidation/annealing above T_g, however, causes new phase(s) to develop, increasing ARM by several orders of magnitude, but also having a much lower blocking temperatures, indicating the predominance of a high-Ti phase, unlike that found in SBG used in magnetic experiments.

[54] Amorphous metastable phase separation and concomitant segregation of Ti into a single liquid, while Fe would be present in both undercooled liquids, could lead to the nucleation of ferrites with a broad range of Fe/Ti; the presence of such grains in experimental as-quenched glass, low-T oxidized glass and natural SBG lends weight to the idea that such phase separation is the mechanism by which the compositional range is produced.

Acknowledgments

[55] We thank Tony McCormick and Joe Devine, both of Brown University, for help with the TEM and microprobe work, respectively. The manuscript was improved thanks to the careful formal reviews by Don Dingwell, Anne Pommier, Rob Van der Voo, and Jim Tyburczy. This work was supported financially, in part, by the National Science Foundation Program in Geophysics, grants EAR-0538170 (to R.F.C.) and EAR-0537981 (to J.S.G.). This is Institute for Rock Magnetism contribution 1005.

References

Andreev, N. S., E. A. Porai-Koshits, and O. Z. Mazurin (1984), Methods of studying metastable phase separation, in *Phase Separation in Glass*, edited by O. Z. Mazurin and E. A. Porai-Koshits, pp. 67–102, Elsevier, Amsterdam.

Asimow, P. D., and M. S. Ghiorso (1998), Algorithmic modifications extending MELTS to calculate subsolidus phase relations, *Am. Mineral.*, *83*(9–10), 1127–1132.

Beall, G. H., and H. L. Rittler (1976), Basalt glass ceramics, *Am. Ceram. Soc. Bull.*, *55*(6), 579–582.

Bowles, J., J. S. Gee, D. V. Kent, E. Bergmanis, and J. Sinton (2005), Cooling rate effects on paleointensity estimates in submarine basaltic glass and implications for dating young flows, *Geochem. Geophys. Geosyst.*, *6*, Q07002, doi:10.1029/2004GC000900.

Bowles, J., J. S. Gee, D. V. Kent, M. R. Perfit, S. A. Soule, and D. J. Fornari (2006), Paleointensity applications to timing and extent of eruptive activity, 9°–10°N East Pacific Rise, *Geochem. Geophys. Geosyst.*, *7*, Q06006, doi:10.1029/2005GC001141.

Buddington, A. F., and D. H. Lindsley (1964), Iron-titanium oxide minerals and synthetic equivalents, *J. Petrol.*, *5*(2), 310–357.

Burkhard, D. J. M., and H. Müller-Sigmund (2007), Surface alteration of basalt due to cation-migration, *Bull. Volcanol.*, *69*, 319–328, doi:10.1007/s00445-006-0076-3.

Chakraborty, S. (1995), Diffusion in silicate melts, *Rev. Mineral. Geochem.*, *32*(1), 411–503.

Chiang, Y.-M., and W. D. Kingery (1983), Spinodal decomposition in a K_2O-Al_2O_3-CaO-SiO_2 glass, *J. Am. Ceram. Soc.*, *66*(9), c171–c172, doi:10.1111/j.1151-2916.1983.tb10632.x.

Christie, D. M., I. S. E. Carmichael, and C. H. Langmuir (1986), Oxidation states of mid-ocean ridge basalt glasses, *Earth Planet. Sci. Lett.*, *79*, 397–411, doi:10.1016/0012-821X(86)90195-0.

Chu, W.-K., J. W. Mayer, and M.-A. Nicolet (1978), Backscattering Spectrometry, 384 pp., Academic, San Diego, Calif.

Cook, G. B., and R. F. Cooper (1999), Redox dynamics in the high-temperature float processing of glasses. I. Reaction between undoped and iron-doped borosilicate glassmelts and a gold-tin alloy, *J. Non Cryst. Solids*, *249*, 210–227, doi:10.1016/S0022-3093(99)00312-9.

Cook, G. B., and R. F. Cooper (2000), Iron concentration and the physical processes of dynamic oxidation in an alkaline earth aluminosilicate glass, *Am. Mineral.*, *85*, 397–406.

Cooper, R. F., J. B. Fanselow, and D. B. Poker (1996a), The mechanism of oxidation of a basaltic glass: Chemical diffusion of network-modifying cations, *Geochim. Cosmochim. Acta*, *60*(17), 3253–3265, doi:10.1016/0016-7037(96)00160-3.

Cooper, R. F., J. B. Fanselow, J. K. R. Weber, D. R. Merkley, and D. B. Poker (1996b), Dynamics of oxidation of a Fe^{2+}-bearing aluminosilicate (basaltic) melt, *Science*, *274*, 1173–1176, doi:10.1126/science.274.5290.1173.

Cooper, R. F., L. A. Everman, J. W. Hustoft, and S.-H. Shim (2010), Mechanism and kinetics of reduction of a FeO-Fe_2O_3-CaO-MgO aluminosilicate melt in a high-CO-activity environment, *Am. Mineral.*, *95*, 810–824, doi:10.2138/am.2010.3375.

Dingwell, D. B. (1990), Effects of structural relaxation on cationic tracer diffusion in silicate melts, *Chem. Geol.*, *82*, 209–216, doi:10.1016/009-2541(90)90082-I.

Dingwell, D. B. (1992), Density of some titanium-bearing silicate liquids and the compositional dependence of the partial molar volume of TiO_2, *Geochim. Cosmochim. Acta*, *56*(9), 3403–3407, doi:10.1016/0016-7037(92)90387-X.

Dingwell, D. B., and S. L. Webb (1989), Structural relaxation in silicate melts and non-Newtonian melt rheology in geologic processes, *Phys. Chem. Miner.*, *16*(5), 508–516, doi:10.1007/BF00197020.

Dingwell, D., and S. L. Webb (1990), Relaxation in silicate melts, *Eur. J. Mineral.*, *2*(4), 427–449.

Doolittle, L. R. (1985), Algorithms for the rapid simulation of Rutherford backscattering spectra, *Nucl. Instrum. Methods Phys. Res., Sect. B*, *9*(3), 344–351, doi:10.1016/0168-583X(85)90762-1.

Draeger, U., M. Prevot, T. Poidras, and J. Riisager (2006), Single domain chemical, thermochemical and thermal remanences in a basaltic rock, *Geophys. J. Int.*, *166*, 12–32, doi:10.1111/j.1365-246X.2006.02862.x.

Dunlop, D. J., and Ö. Özdemir (1997), *Rock Magnetism: Fundamentals and Frontiers*, 573 pp., doi:10.1017/CBO9780511612794, Cambridge Univ. Press, New York.

Fabian, K. (2009), Thermochemical remanence acquisition in single-domain particle ensembles: A case for possible overestimation of the geomagnetic paleointensity, *Geochem. Geophys. Geosyst.*, *10*, Q06Z03, doi:10.1029/2009GC002420.

Freda, C., D. R. Baker, and P. Scarlato (2005), Sulfur diffusion in basaltic melts, *Geochim. Cosmochim. Acta*, *69*(21), 5061–5069, doi:10.1016/j.gca.2005.02.002.

Ghiorso, M. S., and R. O. Sack (1995), Chemical mass-transfer in magmatic processes 4. A revised and internally consistent thermodynamic model for the interpolation and extrapolation of liquid-solid equilibria in magmatic systems at elevated-temperatures and pressures, *Contrib. Mineral. Petrol.*, *119*(2–3), 197–212, doi:10.1007/BF00307281.

Hammer, J. E. (2006), Influence of fO_2 and cooling rate on the kinetics and energetics of Fe-rich basalt crystallization, *Earth Planet. Sci. Lett.*, *248*, 618–637, doi:10.1016/j.epsl.2006.04.022.

Hayashi, M., M. Susa, and K. Nagata (1999), Magnetic structure of as-quenched silicate glasses containing iron oxides, *J. Appl. Phys.*, *85*(4), 2257–2263, doi:10.1063/1.369535.

Heller, R., R. T. Merrill, and P. L. McFadden (2002), The variation of intensity of Earth's magnetic field with time, *Phys. Earth Planet. Inter.*, *131*, 237–249, doi:10.1016/S0031-9201(02)00038-9.

Henderson, P., J. Nolan, G. C. Cunningham, and R. K. Lowry (1985), Structural controls and mechanisms of diffusion in natural silicate melts, *Contrib. Mineral. Petrol.*, *89*, 263–272, doi:10.1007/BF00379459.

Hormadaly, J. (1986), Empirical methods for estimating the linear coefficient of expansion of oxide glasses from their composition, *J. Non Cryst. Solids*, *79*, 311–324, doi:10.1016/0022-3093(86)90230-9.

Lange, R. A., and I. S. E. Carmichael (1987), Densities of Na_2O-K_2O-CaO-MgO-FeO-Fe_2O_3-Al_2O_3-TiO_2-SiO_2 liquids: New measurements and derived partial molar properties, *Geochim. Cosmochim. Acta*, *51*, 2931–2946, doi:10.1016/0016-7037(87)90368-1.

Leonhardt, R., J. Matzka, A. R. L. Nichols, and D. B. Dingwell (2006), Cooling rate correction of paleointensity determination for volcanic glasses by relaxation geospeedometry, *Earth Planet Sci. Lett.*, *243*, 282–292, doi:10.1016/j.epsl.2005.12.038.

Lowry, R. K., P. Henderson, and J. Nolan (1982), Tracer diffusion of some alkali, alkaline-earth and transition element ions in a basaltic and an andesitic melt, and the implications concerning melt structure, *Contrib. Mineral. Petrol.*, *80*, 254–261, doi:10.1007/BF00371355.

McClelland, E. (1996), Theory of CRM acquired by grain growth, and its implications for TRM discrimination and palaeointensity determination in igneous rocks, *Geophys. J. Int.*, *126*(1), 271–280, doi:10.1111/j.1365-246X.1996.tb05285.x.

McMillan, P. W. (1979), *Glass-Ceramics*, 2nd ed., 285 pp., Academic, London.

Métrich, N., M. Bonnin-Mosbah, J. Susini, B. Menez, and L. Galoisy (2002), Presence of sulfite (S^{IV}) in arc magmas: Implications for volcanic sulfur emissions, *Geophys. Res. Lett.*, *29*(11), 1538, doi:10.1029/2001GL014607.

Minitti, M. E., J. F. Mustard, and M. J. Rutherford (2002), Effects of glass content and oxidation on the spectra of SNC-like basalts: Applications to Mars remote sensing, *J. Geophys. Res.*, *107*(E5), 5030, doi:10.1029/2001JE001518.

Muan, A. (1957), Phase equilibrium relationships at liquidus temperatures in the system FeO-Fe_2O_3-Al_2O_3-SiO_2, *J. Am. Ceram. Soc.*, *40*(12), 420–431, doi:10.1111/j.1151-2916.1957.tb12566.x.

Myers, J., and H. P. Eugster (1983), The system Fe-Si-O-oxygen buffer calibrations to 1,500K, *Contrib. Mineral. Petrol.*, *82*(1), 75–90, doi:10.1007/BF00371177.

Mysen, B., and D. Neuville (1995), Effect of temperature and TiO_2 content on the structure of $Na_2Si_2O_5$—$Na_2Ti_2O_5$ melts and glasses, *Geochim. Cosmochim. Acta*, *59*(2), 325–342, doi:10.1016/0016-7037(94)00290-3.

Mysen, B. O., and P. Richet (2005), *Silicate Glasses and Melts: Properties and Structure*, 544 pp., Elsevier, San Diego, Calif.

Naslund, H. R. (1983), The effect of oxygen fugacity on liquid immiscibility in iron-bearing silicate melts, *Am. J. Sci.*, *283*, 1034–1059.

Nowak, M., D. Porbatzki, K. Spickenbom, and O. Diedrich (2003), Carbon dioxide speciation in silicate melts: A restart, *Earth Planet. Sci. Lett.*, *207*, 131–139, doi:10.1016/S0012-821X(02)01145-7.

O'Horo, M. P., and J. F. O'Neill (1976), Magnetic properties of an iron borosilicate glass, in *Amorphous Magnetism II*, edited by R. A. Levy and R. Hasegawa, pp. 651–662, Plenum, New York.

Paul, A. (1990), Oxidation-reduction equilibrium in glass, *J. Non Cryst. Solids*, *123*(1–3), 354–362, doi:10.1016/0022-3093(90)90808-Y.

Phillips, B., and A. Muan (1959), Phase equilibria in the system CaO-iron oxide-SiO_2 in air, *J. Am. Ceram. Soc.*, *42*(9), 413–423, doi:10.1111/j.1151-2916.1959.tb12966.x.

Philpotts, A. R. (1982), Compositions of immiscible liquids in volcanic rocks, *Contrib. Mineral. Petrol.*, *80*, 201–218, doi:10.1007/BF00371350.

Philpotts, A. R. (2008), Comments on: Liquid immiscibility and the evolution of basaltic magma, *J. Petrol.*, *49*(12), 2171–2175, doi:10.1093/petrology/egn061.

Pick, T., and L. Tauxe (1993), Geomagnetic palaeointensities during the Cretaceous normal superchron measured using submarine basaltic glass, *Nature*, *366*(6452), 238–242, doi:10.1038/366238a0.

Pick, T., and L. Tauxe (1994), Characteristics of magnetite in submarine basaltic glass, *Geophys. J. Int.*, *119*(1), 116–128, doi:10.1111/j.1365-246X.1994.tb00917.x.

Pommier, A., F. Gaillard, and M. Pichavant (2010), Time-dependent changes of the electrical conductivity of basaltic melts with redox state, *Geochim. Cosmochim. Acta*, *74*, 1653–1671, doi:10.1016/j.gca.2009.12.005.

Potuzak, M., A. R. L. Nichols, D. B. Dingwell, and D. A. Clague (2008), Hyperquenched volcanic glass from Loihi Seamount, Hawaii, *Earth Planet. Sci. Lett.*, *270*, 54–62, doi:10.1016/j.epsl.2008.03.018.

Roedder, E. (1978), Silicate liquid immiscibility in magmas and in the system K_2O-FeO-Al_2O_3-SiO_2: An example of serendipity, *Geochim. Cosmochim. Acta*, *42*(11), 1597–1617, doi:10.1016/0016-7037(78)90250-8.

Roselieb, K., and A. Jambon (2002), Tracer diffusion of Mg, Ca, Sr and Ba in Na-aluminosilicate melts, *Geochim. Cosmochim. Acta*, *66*(1), 109–123, doi:10.1016/S0016-7037(01)00754-2.

Schmalzried, H. (1983), Internal and external oxidation of non-metallic compounds and solid solutions (I), *Ber. Bunsenges. Phys. Chem*, *87*, 551–558.

Seward, T. P., III, D. R. Uhlmann, and D. Turnbull (1968), Development of two-phase structure in glasses, with special reference to the system BaO-SiO_2, *J. Am. Ceram. Soc.*, *51*(11), 634–642, doi:10.1111/j.1151-2916.1968.tb12635.x.

Smirnov, A. V., and J. A. Tarduno (2003), Magnetic hysteresis monitoring of Cretaceous submarine basaltic glass during Thellier paleointensity experiments: Evidence for alteration and attendant low field bias, *Earth Planet. Sci. Lett.*, *206*(3–4), 571–585, doi:10.1016/S0012-821X(02)01123-8.

Smith, D. R., and R. F. Cooper (2000), Dynamic oxidation of a Fe^{2+}-bearing calcium-magnesium-aluminosilicate glass: The effect of molecular structure on chemical diffusion and reaction morphology, *J. Non Cryst. Solids*, *278*, 145–163, doi:10.1016/S0022-3093(00)00323-9.

Tauxe, L. (2006), Long-term trends in paleointensity: The contribution of DSDP/ODP submarine basaltic glass collections, *Phys. Earth Planet. Inter.*, *156*, 223–241, doi:10.1016/j.pepi.2005.03.022.

Thompson, A. B., M. Aerts, and A. C. Hack (2007), Liquid immiscibility in silicate melts and related systems, *Rev. Mineral. Geochem.*, *65*(1), 99–127, doi:10.2138/rmg.2007.65.4.

Veksler, I. V., A. M. Dorfman, A. A. Borisov, R. Wirth, and D. B. Dingwell (2007), Liquid immiscibility and the evolution of basaltic magma, *J. Petrol.*, *48*(11), 2187–2210, doi:10.1093/petrology/egm056.

Visser, W., and A. F. Koster van Groos (1979), Phase relations in the system K_2O-FeO-Al_2O_3-SiO_2 at 1 atmosphere with special emphasis on low temperature liquid immiscibility, *Am. J. Sci.*, *279*(1), 70–91.

Watson, E. B. (1976), Two-liquid partition coefficients; experimental data and geochemical implications, *Contrib. Mineral. Petrol.*, *56*, 119–134, doi:10.1007/BF00375424.

Wilding, M., D. Dingwell, R. Batiza, and L. Wilson (2000), Cooling rates of hyaloclastites: Applications of relaxation geospeedometry to undersea volcanic deposits, *Bull. Volcanol.*, *61*(8), 527–536, doi:10.1007/s004450050003.

Yamamoto, Y. (2006), Possible TCRM acquisition of the Kilauea 1960 lava, Hawaii: Failure of the Thellier paleointensity determination inferred from equilibrium temperature of the Fe-Ti oxide, *Earth Planets Space*, *58*(8), 1033–1044.

Zhou, W., R. Van der Voo, D. R. Peacor, and Y. Zhang (2000), Variable Ti-content and grain size of titanomagnetite as a function of cooling rate in very young MORB, *Earth Planet. Sci. Lett.*, *179*, 9–20, doi:10.1016/S0012-821X(00)00100-X.